

Segment diffusion in polymers confined in nanopores: A fringe-field NMR diffusometry study

Elmar Fischer and Rainer Kimmich

Sektion Kernresonanzspektroskopie, Universität Ulm, 89069 Ulm, Germany

Uwe Beginn and Martin Möller

Abteilung Organische Chemie III, Universität Ulm, 89069 Ulm, Germany

Nail Fatkullin

Kazan State University, 420008 Kazan, Tatarstan, Russia

(Received 27 July 1998)

The dynamics of polymer chains confined in artificial tubes formed by the pores of a nanoporous material should display all the features predicted by the reptation model, provided that the polymer/wall interaction does not lead to adsorption effects. We have studied the segment diffusion behavior of linear polyethyleneoxide in the molten state in pores of well characterized cross-linked polyhydroxyethylmethacrylate matrices. These “semi-interpenetrating networks” were prepared in such a way that (10 ± 2) nm thick cylindrical pores completely filled with polyethyleneoxide were produced. The measuring technique was fringe-field NMR diffusometry. The results are compatible with a power law for the mean squared displacement, $\langle r^2 \rangle \propto t^{-0.4 \pm 0.1} M_w^{-0.8 \pm 0.2}$, where t is the diffusion time and M_w is the weight average molecular mass. This is to be compared with the limiting law $\langle r^2 \rangle \propto t^{-1/2} M_w^{-1/2}$ predicted by de Gennes, Doi, and Edwards for region III, that is, $\tau_R \ll t \ll \tau_d$ of the tube/reptation model. In the frame of the experimental accuracy the conclusion is that the reptative diffusion mechanism applies to linear polymer chains of sufficient length relative to the diameter of the confining pores. [S1063-651X(99)01404-X]

PACS number(s): 66.10.Cb, 61.25.Hq, 81.05.Rm, 81.05.Ys

I. INTRODUCTION

Transport processes of polymers in porous materials are of interest for techniques like membrane filtering, chromatography, or the production of advanced materials with tailored properties. The central question is how chain dynamics changes if the motion of the polymer is impeded by solid obstacles.

In his famous 1971 reptation paper, de Gennes treated the dynamics of polymer chains in the presence of fixed obstacles [1]. Doi and Edwards [2] extended the theory and derived a number of limiting power laws for segment and center-of-mass diffusion. In this model, polymer chains are assumed to be confined in tubes having a Gaussian conformation statistics. The tube diameter a as a free parameter is limited by $d \ll a \ll L$ where d is the chain diameter and L the chain length. The mean squared segment displacement is predicted to obey the following limiting laws as concerns the dependences on the diffusion time t and the number of Kuhn segments per chain, N :

$$\text{limit I: } \langle r^2 \rangle \propto N^0 t^{1/2} \quad \text{for } t \ll \tau_e, \quad (1)$$

$$\text{limit II: } \langle r^2 \rangle \propto N^0 t^{1/4} \quad \text{for } \tau_e \ll t \ll \tau_R, \quad (2)$$

$$\text{limit III: } \langle r^2 \rangle \propto N^{-1/2} t^{1/2} \quad \text{for } \tau_R \ll t \ll \tau_d, \quad (3)$$

$$\text{limit IV: } \langle r^2 \rangle \propto N^{-2} t \quad \text{for } t \gg \tau_d. \quad (4)$$

The characteristic time constants τ_e , τ_R , and τ_d are the “entanglement time,” the “Rouse relaxation time,” and the “tube disengagement time,” respectively.

Reptation of polymer chains in tubes defined by heterogeneous matrices such as porous glass, gels, and membranes has been examined in the literature using various experimental techniques [3–10]. Computer simulations of chain dynamics in tubes are reported in Refs. [11–15]. In the latter studies reptational motion either was already anticipated as an element of the simulation algorithm, or was treated as a result of the excluded-volume interaction. In other terms, the chains can only move in the free pore space.

The objective of the present study is to mimic the tube (or the “fixed obstacles” according to de Gennes’s original terminology) by semi-interpenetrating networks. That is, linear polymers are confined in a matrix also of an organic polymer nature. Ideally one would like to study free polymers in networks formed of the same polymer species. This is in contrast to attempts to study confinement effects by incorporating organic polymers into nanoporous silica glasses [3,5,7,9,10]. With the latter experiments the interpretation difficulty arises as to how to reliably distinguish adsorption from geometrical restriction effects. The bicontinuous semi-interpenetrating networks to be described in the following are much less prone to the influence of adsorption on the dynamics of the incorporated linear polymer chains. Furthermore, no problem arises in imbibing the porous medium with the polymers of interest, because the samples are prepared with the diffusing species, which are *a priori* incorporated in the host material.

As a suitable investigation method we rely on fringe-field NMR diffusometry [16]. The solid matrix has a proton transverse relaxation time more than one order of magnitude shorter than that of the incorporated melt of linear polymers. The signals of the two components therefore can easily be

distinguished, and the selective determination of displacements of the incorporated mobile chains becomes feasible.

II. SAMPLES AND METHODS

A. Semi-interpenetrating networks

Interpenetrating networks are defined as mixtures of two or more polymer components one or more of which are cross-linked [17,18]. A “semi-interpenetrating network” (semi-IPN) is formed by two polymer species, one of which is crosslinked. The morphology of such systems has only recently been explored by de Graaf *et al.* [19].

Linear polyethyleneoxide (PEO) fractions of well defined molecular weight were dissolved in a mixture consisting of 80% hydroxyethylmethacrylate and 20% ethylene glycol dimethacrylate at 60 °C. These ternary solutions were quenched into the spinodal decomposition region, so that thin polyethyleneoxide cylinders were formed with diameters growing with time. The demixing process was stopped by vitrification of the polymer below the glass transition where molecular motions virtually freeze in. That is, at this stage of the procedure the samples consisted of thermoreversible “networks.”

Polymerizing and cross-linking the hydroxyethylmethacrylate monomers in the frozen state by UV irradiation produces a semi-IPN of linear polyethyleneoxide confined in thin channels in the polyhydroxyethylmethacrylate (PHEMA) network. That is, even above the melting point of the polyethyleneoxide the original morphology produced by the spinodal decomposition is preserved.

Samples were prepared using four different polyethyleneoxide fractions, $M_w = 6000$, 11 600, 22 500, and 41 500, purchased from Polymer Standard Service, Mainz. The polydispersities were specified as 1.03, 1.04, 1.06, and 1.14, respectively. The hot solutions (60 °C) were quenched between precooled polyethylene plates which were in contact with a cold aluminum block kept at a temperature of -180 °C. This produces 0.5 mm thick solid films which were subsequently heated to -50 °C. At this temperature the polymerization/cross-linking reaction has been performed using UV light of a 366 nm UV lamp.

The resulting PHEMA pore diameters were characterized by electron microscopy, small-angle x-ray scattering, as well as spin-diffusion measurements. Coincidentally the pore diameter was estimated to be $d_p = (10 \pm 2)$ nm independent of molecular weight of the polyethyleneoxide. The pores are of a cylindrical shape as expected for spinodal decomposition.

This can be visualized by transmission electron microscopy (TEM). A typical micrograph acquired with one of our samples is shown in Fig. 1. The freeze-fractured sample surfaces were decorated with metal particles under an angle much smaller than 90°. The resulting image contrasts then display the surface topology. Pore channels in the fracture plane show up as elevations or depressions. Assuming that the channels visible in the image plane have no branches in the missing third dimension permits one to estimate a minimum length between neighboring branches in the order of 100 nm. No such structures could be observed with a replica of the pure matrix prepared without PEO, but otherwise in just the same way. The shape of the channels appears to have a random character. An analysis in terms of a statistical

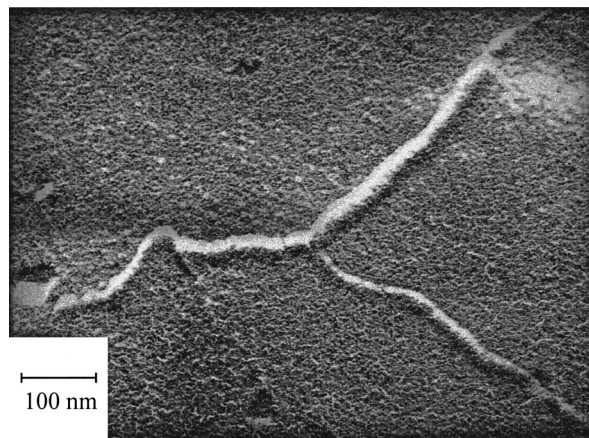


FIG. 1. Typical TEM micrograph of a replica of a freeze-fractured surface of polyethyleneoxide $M_w = 6000$ in PHEMA. The sample was freeze fractured and subsequently covered with a 2.5 nm layer of platinum under an angle of 37°. The metal film was afterwards sustained with a 25 nm thick carbon layer. The whole film was dissolved from the surface with a concentrated aqueous NaOH solution and transferred to copper grids. Magnification: $\times 100\,000$.

evaluation fails, however, because of the limited number of identifiable objects and the fact that no three-dimensional reproduction is possible in this way. We plan to publish a detailed description of the preparation and characterization procedure in the future [20].

B. Instruments and measuring technique

Fringe-field proton diffusometry was employed using a 9.4 T Bruker wide-bore magnet. The fringe-field gradient was 60 T/m at 200 MHz proton resonance. Reference experiments were carried out at the same frequency using the same radio frequency (rf) console in the homogeneous central field of a Biospec 4.7 T magnet. Details of the method taking into account the dipolar correlation effect [21,22] relevant here are described in Ref. [23]. Stimulated echoes were recorded using the standard rf pulse sequence

$$\frac{\pi}{2} - \tau_1 - \frac{\pi}{2} - \tau_2 - \frac{\pi}{2} - \tau_1 - (\text{stimulated echo}). \quad (5)$$

In the experiments, the interval τ_1 was varied, whereas $\tau_2 \gg \tau_1$ was kept constant. The stimulated-echo amplitudes were normalized to the limit $\tau_1 \rightarrow 0$ in each case. The quotient of the normalized echo amplitudes recorded for the same pulse intervals as a function of τ_1 with and without field gradient then gives the attenuation curve due to translational diffusion. All measurements were performed at a temperature of (80 ± 1) °C. At this temperature the proton transverse relaxation time of the PHEMA matrix is on the order of 40 μs , i.e., the matrix echo signals can safely be neglected relative to those of PEO, which were recorded with a first pulse interval incremented beginning with $\tau_1 \geq 120$ μs .

In the limit of long diffusion times relative to the encoding gradient intervals, $t \gg \tau_1$, the echo attenuation by diffusion can be represented by

$$E_d(q, t) = \langle \exp\{iqz(t)\} \rangle. \quad (6)$$

In fringe-field experiments, the field gradient is directed along the z axis. The displacement component along the gradient direction is represented by $z(t)$, the “wave number” by $q = \gamma G \tau_1$, where γ is the gyromagnetic ratio and G is the gradient strength. The angle brackets in Eq. (6) indicate the ensemble average formed with the aid of the probability density for displacements $z(t)$ in the diffusion time t (which essentially is equal to the pulse interval τ_2 under the present conditions). No assumption concerning a potentially Gaussian character of this probability density has been made.

The experimental echo attenuation curves were evaluated in two ways. Apart from the “exact” formalism anticipating the tube/reptation model (see Ref. [24]), the following approach was employed. Expanding Eq. (6) and taking the limit for small q values leads to the approximate expressions

$$E_d(q, t) \approx 1 - \frac{q^2}{2} \langle z^2(t) \rangle \approx \exp\left\{-\frac{q^2}{2} \langle z^2(t) \rangle\right\}. \quad (7)$$

The exponent is obviously dominated by the second moment of the probability density. Formally equating this quantity with the result expected for a Gaussian probability density leads to

$$\langle z^2(t) \rangle = 2\tilde{D}t, \quad (8)$$

where \tilde{D} is the effective and potentially time dependent diffusion coefficient which is defined in this way. The echo attenuation function can then be rewritten for small q values as

$$E_d(q, t) \approx \exp\{-q^2\tilde{D}t\}. \quad (9)$$

That is, plots of $\ln E_d(q, t)$ versus q^2 are expected to reveal straight lines in the limit of sufficiently small q values. Note, however, that the attenuation curves deviate from straight lines at large wave numbers whenever the probability density deviates from a Gaussian distribution. The segment diffusion by reptation is intrinsically connected with non-Gaussian propagators [24]. Only at very long diffusion times when center-of-mass diffusion dominates [limit IV given in Eq. (4)] does polymer diffusion become normal in the sense that a Gaussian displacement distribution applies. In that case the effective segment diffusion coefficient \tilde{D} approaches the center-of-mass self-diffusion coefficient D_c .

III. RESULTS

Figure 2 shows the center-of-mass self-diffusion coefficient $\tilde{D} = D_c$ of the bulk melts at 80 °C as a function of molecular weight. The data have been evaluated by fitting a Gaussian to the echo attenuation curves. In this case, the Gaussian behavior of the propagator is well fulfilled because the diffusion time is much longer than the disengagement time τ_d . For instance, τ_d is expected to be about 0.5 ms for $M_w = 41\,500$ whereas $\tau_2 \geq 100$ ms. The well known inverse square proportionality $D_c \propto M^{-2}$ expected for molecular weights above the critical value [25] $M_c = 3600$ is represented by the solid line.

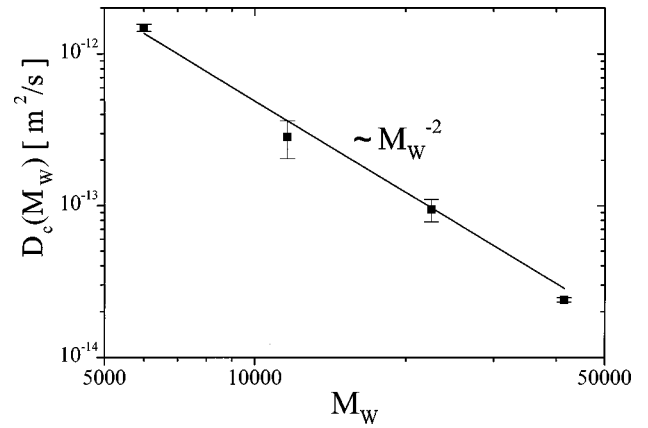


FIG. 2. Center-of-mass self-diffusion coefficient in bulk polyethyleneoxide melts as a function of molecular weight at 80 °C. The solid line displays the power law $D_c \propto M^{-2}$. $\tau_2 \geq 100$ ms.

The diffusion behavior changes significantly when the PEO chains are confined in the semi-interpenetrating networks. Figures 3–6 show typical echo attenuation curves for different diffusion times τ_2 at 80 °C as a function of q^2 . The non-Gaussian character of the attenuation curves is obvious. A steep initial decay at small q values is followed by a more slowly decaying section at high q values. For $M_w = 6000$, the slowly decaying component comprises about 50% of the signal whereas for all other molecular weights investigated in this study the slowly decaying component turned out to be larger than 80%.

Evaluating the initial steep decays for the effective diffusion coefficient one finds values which are close to those of the bulk melt. This initial attenuation is considered to be due to pore channels aligned along the field gradient so that the confinement does not matter. In the context of this study, this component therefore is of no interest. By contrast, the slowly decaying (and dominating) part of the attenuation curves reflects the dynamics of chains experiencing the pore confinements in full.

The effective diffusion coefficient was evaluated according to Eq. (9) from the initial part of the slowly decaying echo attenuation component. The results are displayed in Figs. 7 and 8. In the diffusion time interval from 10 to 200

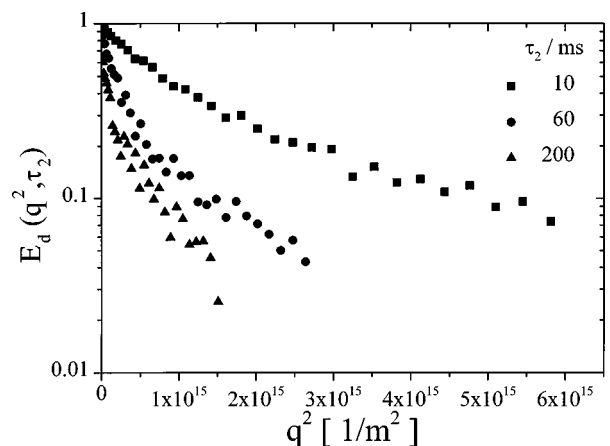


FIG. 3. Diffusional attenuation curves of polyethyleneoxide $M_w = 6000$ confined in PHEMA as a function of q^2 for different diffusion times at 80 °C.

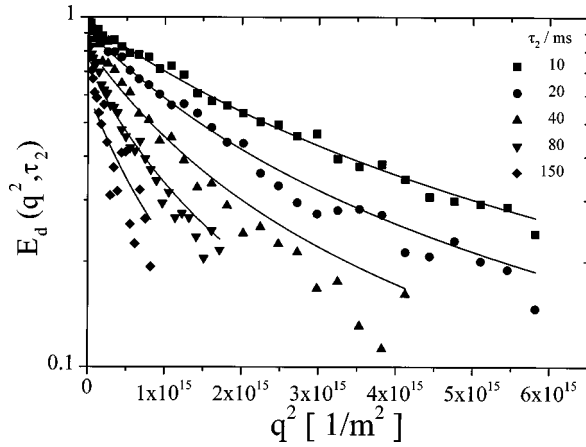


FIG. 4. Diffusional attenuation curves of polyethyleneoxide $M_w = 11\,600$ confined in PHEMA as a function of q^2 for different diffusion times at $80\text{ }^\circ\text{C}$. The solid lines represent a fit of Eq. (14) to the experimental data. The tube diameter as the only fitting parameter is found to be $a = (7.0 \pm 0.5)\text{ nm}$.

ms, the effective diffusion coefficient turned out to be time dependent. Unfortunately, the limited dynamical range available in these experiments does not permit the unambiguous conclusion that a power law applies. It can, however, be stated that the data can be described in the frame of the experimental range and accuracy by

$$\bar{D} \propto N^{-0.8 \pm 0.2} t^{-0.4 \pm 0.1}. \quad (10)$$

These chain length and time dependences substantially deviate from the behavior observed in the bulk (see Fig. 2).

IV. INTERPRETATION

The data for the effective diffusion coefficient suggest an anomalous mean squared displacement obeying

$$\langle r^2(t) \rangle \propto N^{-0.8 \pm 0.2} t^{0.6 \pm 0.1} \quad (11)$$

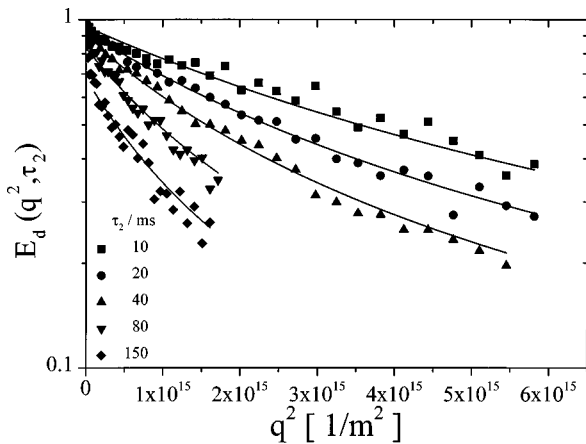


FIG. 5. Diffusional attenuation curves of polyethyleneoxide $M_w = 22\,500$ confined in PHEMA as a function of q^2 for different diffusion times at $80\text{ }^\circ\text{C}$. The solid lines represent a fit of Eq. (14) to the experimental data. The tube diameter as the only fitting parameter is found to be $a = (6.0 \pm 0.5)\text{ nm}$.

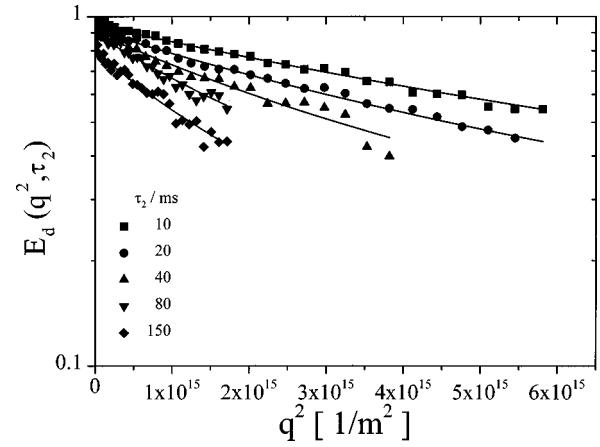


FIG. 6. Diffusional attenuation curves of polyethyleneoxide $M_w = 41\,500$ confined in PHEMA as a function of q^2 for different diffusion times at $80\text{ }^\circ\text{C}$. The solid lines represent a fit of Eq. (14) to the experimental data. The tube diameter as the only fitting parameter turned out to be $a = (4.5 \pm 0.5)\text{ nm}$.

in reasonable coincidence with the predictions for the tube/reptation model given in Eq. (3) for limit III, i.e., $\tau_R \ll t \ll \tau_d$. This is the regime in which the whole chain coherently diffuses along the tube.

The fact that the data are largely dominated by this particular limit indicates that the “disengagement time” τ_d is particularly long in the present situation. In other words, the special preparation technique of the semi-interpenetrating networks leads to channels with minor branching (compare Fig. 1). A polymer chain confined into such channels has little chance to leave the original tube. Even after a long time a finite chance remains to return to the original position.

On the other hand, the (longest) Rouse relaxation time τ_R is relatively short due to the moderate chain lengths used in this study. That is, the diffusion time range probed in our experiments virtually is within limit III. Some minor deviations can merely be stated for polyethyleneoxide with $M_w = 11\,600$ at diffusion times longer than $\approx 80\text{ ms}$ (see Fig. 7). This may be interpreted as the crossover to limit IV [see Eq. (4)] where center-of-mass diffusion dominates.

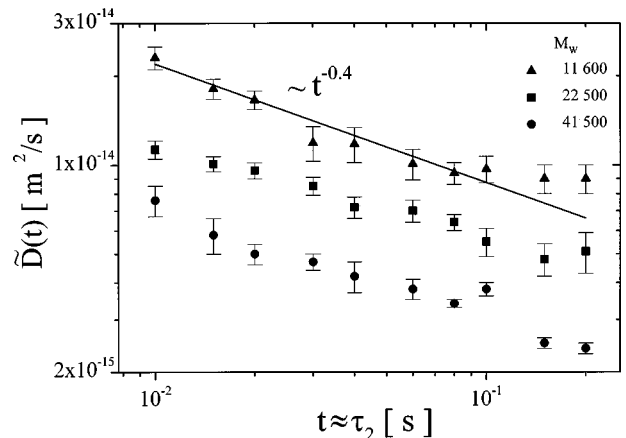


FIG. 7. Effective diffusion coefficient of polyethyleneoxide confined in PHEMA at $80\text{ }^\circ\text{C}$ as a function of the diffusion time τ_2 . The curve parameter is the molecular weight. The solid line represents a power law $\bar{D} \propto t^{-0.4}$.

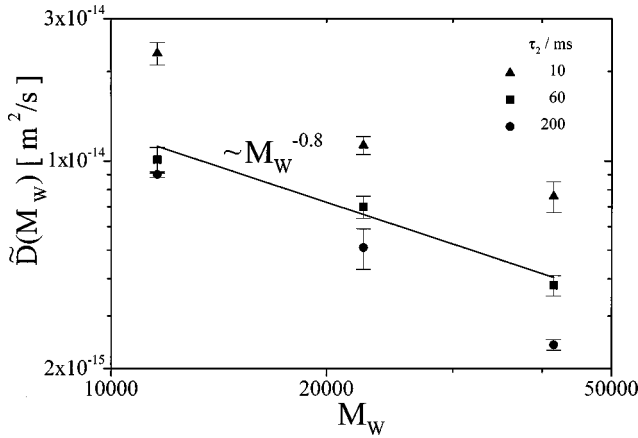


FIG. 8. Effective diffusion coefficient of polyethyleneoxide confined in PHEMA at 80 °C as a function of molecular weight. The curve parameter is the molecular weight. The solid line represents the power law $\bar{D} \propto M^{-0.8}$.

The echo attenuation data given in Figs. 3–6 were also evaluated utilizing a formalism specifically developed for limits II–IV of the tube/reptation model [24]. The echo attenuation factor for reptation reads

$$E_d(q^2, t) = \exp\left\{\frac{q^4 a^2 \langle s^2(t) \rangle}{72}\right\} \operatorname{erfc}\left\{\frac{q^2 a \sqrt{\langle s^2(t) \rangle}}{6\sqrt{2}}\right\} \times \exp\{-q^2 D t\} \quad (12)$$

with the mean squared displacement along the curvilinear path [2]

$$\langle s^2(t) \rangle = \frac{2D_0 t}{N + 12a^2 D_0 t / N^2 b^4} + \frac{2b\sqrt{D_0 t}}{\sqrt{3\pi + 18\sqrt{D_0 t} / Nb}}. \quad (13)$$

The quantities b and D_0 are the Kuhn segment length and the Kuhn segmental diffusivity, respectively. The diffusion time t can be equated with τ_2 in the limit $\tau_2 \gg \tau_1$ which is well fulfilled in all experiments reported here. Equation (12) may be approximated for limit III (which solely matters in our case) by

$$E_d(q^2, t) \approx \exp\left\{\frac{q^4 a^2 D_0 t}{36N}\right\} \operatorname{erfc}\left\{\frac{q^2 a \sqrt{D_0 t}}{6\sqrt{N}}\right\}. \quad (14)$$

In this expression, the tube diameter a is the only free fitting parameter (apart from a normalization constant). The number of Kuhn segments per chain, N , the Kuhn segmental

length b , and the Kuhn segment diffusivity D_0 were estimated using literature data [25,26] for the bulk melt assuming that these parameters are not affected by the artificial pore confinement. The values are $N = M_w/85.3$, $D_0 = 9.66 \times 10^{-10} \text{ m}^2/\text{s}$, and $b = 8.38 \text{ nm}$.

Equation (14) was fitted to the echo attenuation data independently for each molecular weight studied here. The resulting parameter values are given in Table I. With PEO 6000, no reasonable fit was possible. The tube diameters fitted to the data of the other samples range from 4.5 to 7 nm. That is, the values obtained in this way are of the same order of magnitude as the PHEMA channel diameter which was evaluated with various independent methods to be $(10 \pm 2) \text{ nm}$ as described before.

The plateau of the effective diffusion coefficient of PEO 11 600 (see Fig. 7) can be explained as a crossover to limit IV of the tube/reptation model [see Eq. (4)]. The polymer is then assumed to have traveled across many randomly oriented branches within the pore network. In the present case the disengagement time can be interpreted as the time needed to reach the nearest branching point of the PHEMA channels. The curvilinear mean squared displacement can be calculated for limit III as

$$\langle s^2(t) \rangle = 2D_0 N^{-1} t \approx 1.1 \mu\text{m}^2. \quad (15)$$

From the mean curvilinear displacement, one derives the mean squared segment displacement in Euclidian space according to Ref. [2],

$$\langle r^2(t) \rangle = a \sqrt{\langle s^2(t) \rangle} = a \sqrt{2D_0 t / N}. \quad (16)$$

With $a = 7.0 \text{ nm}$, $D_0 = 9.66 \times 10^{-10} \text{ m}^2/\text{s}$, $N = 136$, and $t = 80 \text{ ms}$, we find $\sqrt{\langle r^2(t) \rangle} = 86 \text{ nm}$, a value which is of the same order as the 100 nm estimated from the TEM micrographs (see Fig. 1).

V. DISCUSSION AND CONCLUSIONS

The time and molecular-weight dependences of segment diffusion in linear polyethyleneoxide melts confined to 10 nm channels in a crosslinked PHEMA matrix were examined using fringe-field NMR diffusometry. Beginning with a PEO molecular weight of 11 600, the root mean squared end-to-end distance exceeds the pore diameter (see Table I), so that a real confinement effect on a molecular length scale could be expected for most of the PEO component. With these polymers subject to confinements merely a minor echo signal fraction (less than 20%) behaved as in the bulk, that is, decayed rapidly with a diffusivity corresponding to the bulk value. This signal contribution may be attributed to channels

TABLE I. Characteristics of the PEO/PHEMA samples.

Molecular weight M_w	Number of Kuhn segments N	End-to-end distance $\sqrt{R^2} = \sqrt{Nb^2}$	Fitted tube diameter a
6000.	71	7.0	
11 600.	136	9.8	7.0
22 500.	256	13.4	6.0
41 500.	494	18.5	4.5

parallel to the gradient direction and/or to larger compartments in the PHEMA matrix which may occur due to imperfections of the preparation procedure. All diffusivity data discussed here therefore refer to the slowly decaying signal component arising from the confined part of the linear polymer chains.

Two evaluation protocols were employed. First, an effective, i.e., time dependent, diffusion coefficient was determined from the initial part of the echo attenuation curve. This approach suggests time and molecular-weight dependences in reasonable agreement with the limit III predictions of the tube/reptation model. That is, the “tube” fictitiously introduced in this model can be identified with the real pore channels formed in the semi-interpenetrating networks examined in this study. The time/molecular-weight scale where region III of the tube/reptation model showed up as well as the absolute values of the diffusivities which turned out to be reduced by one order of magnitude indicate a substantially different dynamic situation in the confined melt relative to the bulk.

The question of the length and curvature of the cylindrical pores in the PHEMA matrix may be discussed for the following limits. If the pores were infinitely long and completely straight, Rouse-like behavior [27] would be expected, i.e., $\bar{D} \propto t^0$ and $\bar{D} \propto M^{-1}$. In case the pores again were infinitely long but had a curvature according to Gaussian conformation statistics one would expect $\bar{D} \propto t^{-1/2}$ and $\bar{D} \propto M^{-1/2}$ [see Eq. (16)]. The experimental findings of this study suggest a situation in between these two limits so far as it can be judged on the basis of the restricted molecular-weight range examined. Actually, the disengagement time concluded from the plateau crossover of the effective diffu-

sivity of PEO 11 600 suggests a pore branching point distance of the same order as evaluated from the TEM micrographs so that the assumption of “infinitely” long tubes is justified as far as much shorter root mean squared displacements are considered.

The second evaluation procedure referred to a formalism anticipating the applicability of the tube/reptation model [24]. In this case the whole q and τ_2 ranges explored were taken into account at one time. The fitted tube diameter a turned out to decrease with increasing molecular weight. This finding may reflect the fact that the evaluation formula anticipates a dependence $\bar{D} \propto aN^{-1/2}$ whereas the experimental data suggest $\bar{D} \propto N^{-0.8 \pm 0.2}$.

In this context the question arises as to whether adsorption to the surface plays a role. In this case, the PEO layer adsorbed to the surface would not take part in the diffusion process so that only chains situated in the central part of the channels would contribute to the displacements examined. That is, the effective tube diameter would then be expected to be smaller than suggested by the pore channel dimension. The thickness of the adsorption layer would then vary with the chain length inversely to the effective tube diameter. It is planned to elucidate this question in forthcoming studies employing chemical surface modifications.

ACKNOWLEDGMENTS

We thank Dr. T. Pieper, Dr. F. Mellinger, and Dr. S. Hafner for carrying out the characterization experiments of the PHEMA channels. This work was supported by the Deutsche Forschungsgemeinschaft and the Volkswagen Foundation.

-
- [1] P. G. de Gennes, *J. Chem. Phys.* **55**, 572 (1971).
 [2] M. Doi and S. F. Edwards, *The Theory of Polymer Dynamics* (Clarendon Press, Oxford, 1986).
 [3] W. D. Dozier, J. M. Drake, and J. Klafter, *Phys. Rev. Lett.* **56**, 197 (1986).
 [4] M. P. Bohrer, L. J. Fetters, N. Grizzuti, D. S. Pearson, and M. V. Tirrell, *Macromolecules* **20**, 1827 (1987).
 [5] M. T. Bishop, K. H. Langley, and F. E. Karasz, *Macromolecules* **22**, 1220 (1989).
 [6] J. Käs, H. Strey, and E. Sackmann, *Nature (London)* **368**, 227 (1994).
 [7] S. Stapf and R. Kimmich, *Macromolecules* **29**, 1638 (1996).
 [8] M. Appel and G. Fleischer, *Europhys. Lett.* **40**, 685 (1996).
 [9] W. Gorbatschow, M. Arndt, R. Stannarius, and F. Kremer, *Europhys. Lett.* **35**, 719 (1996).
 [10] L. Petychakis, G. Floudas, and G. Fleischer, *Europhys. Lett.* **40**, 685 (1997).
 [11] R. Kimmich and W. Doster, *J. Polym. Sci., Polym. Phys. Ed.* **14**, 1671 (1976).
 [12] M. Sahimi and V. L. Jue, *Phys. Rev. Lett.* **62**, 629 (1989).
 [13] M. Muthukumar and A. Baumgärtner, *Macromolecules* **23**, 1937 (1989).
 [14] H. Yoon and J. M. Deutsch, *J. Chem. Phys.* **102**, 9090 (1995).
 [15] V. Yamakov, D. Stauffer, A. Milchev, G. M. Foo, and R. B. Pandey, *Phys. Rev. Lett.* **79**, 2356 (1997).
 [16] R. Kimmich, *NMR Tomography, Diffusometry, Relaxometry* (Springer-Verlag, Berlin, 1997).
 [17] J. R. Millar, *J. Chem. Soc. (London), Part I*, 1311 (1960).
 [18] J. R. Millar, D. G. Smith, and W. E. Marr, *J. Chem. Soc. (London), Part II*, 1789 (1962).
 [19] L. A. de Graaf, P.-J. W. Albers, and M. Möller, *J. Polym. Sci., Part B: Polym. Phys.* **34**, 1893 (1996).
 [20] U. Beginn, E. Fischer, T. Pieper, F. Mellinger, M. Möller, and R. Kimmich (unpublished).
 [21] R. Kimmich, E. Fischer, P. T. Callaghan, and N. Fatkullin, *J. Magn. Reson., Ser. A* **117**, 53 (1995).
 [22] F. Grinberg and R. Kimmich, *J. Chem. Phys.* **103**, 365 (1995).
 [23] E. Fischer, R. Kimmich, and N. Fatkullin, *J. Chem. Phys.* **106**, 9883 (1997).
 [24] N. Fatkullin and R. Kimmich, *Phys. Rev. E* **52**, 3273 (1995).
 [25] W. W. Graessley and S. F. Edwards, *Polymer* **22**, 1329 (1981).
 [26] G. D. Smith, D. Y. Yoon, R. L. Jaffe, R. H. Colby, R. Krishnamoorti, and L. J. Fetters, *Macromolecules* **29**, 3462 (1996).
 [27] P. E. Rouse, *J. Chem. Phys.* **21**, 1272 (1953).